Stephen C. Warren-Smith, Kay Schaarschmidt, Mario Chemnitz, Erik P. Schartner, Henrik Schneidewind, Heike Ebendorff-Heidepriem and Markus A. Schmidt

Tunable multi-wavelength third-harmonic generation using exposed-core microstructured optical fiber

Optics Letters, 2019; 44(3):626-629

Published version: http://dx.doi.org/10.1364/OL.44.000626

Tunable multi-wavelength third harmonic generation using exposed-core microstructured optical fiber

STEPHEN C. WARREN-SMITH,[1,2,*] KAY SCHAARSCHMIDT,[1,3] MARIO CHEMNITZ,[1,3] ERIK P. SCHARTNER,[2] HENRIK SCHNEIDEWIND,[1] HEIKE EBENDORFF-HEIDEPRIEM[2], AND MARKUS A. SCHMIDT[1,3,4]

[1]*Leibniz Institute of Photonic Technology (IPHT), Albert-Einstein-Straße 9, 07745 Jena, Germany*
[2]*School of Physical Sciences and ARC Centre of Excellence for Nanoscale BioPhotonics (CNBP) and Institute for Photonics and Advanced Sensing (IPAS), The University of Adelaide, Adelaide, SA 5005, Australia*
[3]*Abbe Center of Photonics, Friedrich Schiller University Jena, Max-Wien-Platz 1, 07743 Jena, Germany*
[4]*Otto Schott Institute of Materials Research (OSIM), Friedrich Schiller University of Jena, Fraunhoferstrasse 6, 07743 Jena, Germany*
**Corresponding author: stephen.warrensmith@adelaide.edu.au*

Received XX Month XXXX; revised XX Month, XXXX; accepted XX Month XXXX; posted XX Month XXXX (Doc. ID XXXXX); published XX Month XXXX

We demonstrate that exposed-core microstructured optical fibers offer multiple degrees of freedom for tailoring third harmonic generation, through core diameter, input polarization, and nanofilm deposition. Varying these parameters allows control of the phase-matching position between an infrared pump wavelength and the generated visible wavelengths. In this work we show how increasing the core diameter over previous experiments (2.57 μm compared to 1.85 μm) allows the generation of multiple wavelengths, which can be further controlled by rotating the input pump polarization and the deposition of dielectric nanofilms. This can lead to highly tailorable light sources for applications such as spectroscopy or nonlinear microscopy.

http://dx.doi.org/10.1364/OL.99.099999

Microstructured optical fibers consist of air holes that run along their length, which provide guidance either through a form of total internal reflection or interference/bandgap effects. Their tailorable geometry and high refractive index contrast between glass and air has allowed them to be designed for diverse applications, such as sensing and nonlinear optics. For nonlinear light generation, suspended-core microstructured optical fibers (SCFs) are particularly attractive due to their ability to guide light with wavelength-scaled core diameters [1, 2]. Core diameters as small as 400 nm have been achieved using soft glass [3] and 800 nm using silica glass [4]. They have been used to demonstrate a variety of nonlinear effects, such as supercontinuum generation [5-7] and four-wave mixing [8-10].

In this work, we consider using solid-core fibers for third harmonic generation (THG). In this process, three photons, typically at an infrared (IR) wavelength, are converted to a single, visible wavelength photon.

THG in waveguides is optimized when the phase of the different waves are matched, which can be achieved in optical fibers by using intermodal phase-matching to overcome material dispersion. That is, the fundamental mode at the infrared wavelength is phase-matched (has the same effective index) to a higher-order mode at one-third of the infrared wavelength. High index contrast waveguides are essential for phase-matching to occur as a sufficient number of higher order modes must be present, while it is known that phase-matching is very sensitive to the waveguide properties [11]. This has previously been shown in configurations such as tapers [12-14], suspended-core fibers [15, 16], and highly doped step-index fibers [17, 18].

Recent research has focused on designing and demonstrating methods for tuning the phase matching conditions, such as controlling the pressure of argon gas either surrounding sub-micron tapers [19] or filled into hollow-core photonic crystal fiber [20], or controlling the pump power to tune the nonlinear phase shift [21]. There is also interest in producing the third harmonic (TH) in fundamental or Gaussian-like modes, rather than multi-lobed higher order modes. This has been theoretically proposed using schemes such as pulse-induced quasi-phase matching in tapered microfibers [22] and dual bandgap photonic crystal fiber structures [23]. Cavanna *et al.* demonstrated that this could be achieved using a hybrid fiber structure combining a photonic bandgap microstructure contained within an index guiding structure [24]. However, such hybrid fiber structures put huge demands on both fiber design and drawing conditions and more practical generation schemes for efficient and tunable THG are desired.

We have recently demonstrated a proof-of-concept that third harmonics can be generated using a variant of the suspended-core

fiber where part of the core is exposed to the external environment on one side [25], termed the exposed-core fiber (ECF) [26-28]. We then demonstrated that the TH generated wavelength could be tuned by depositing dielectric nanofilms onto the open core of the ECF [29].

In this letter, we demonstrate that by combining multiple tuning schemes, including core diameter, input polarization and deposition of high refractive index nanofilms, THG in ECFs can be tailored to produce a rich variety of generated wavelengths spanning almost 100 nm. This provides a pathway towards ultra-fast light sources with defined multi-wavelength TH-emission for applications in sensing, microscopy, and quantum technology.

The fused silica ECF used in our experiments was fabricated using an ultrasonic drilled preform that was then drawn into a fiber in a two-step process, as detailed previously [28], and is shown in Fig. 1. The fiber has an outer diameter of 220 μm (Fig. 1a) and an effective core diameter of 2.57 μm (Fig. 1b).

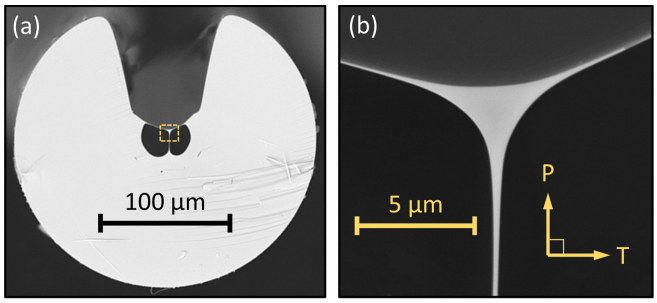

Fig. 1. Scanning electron microscope (SEM) images of the exposed-core microstructured optical fiber (core diameter: 2.57μm). (a) Fiber cross section. (b) Core region. The arrows in (b) define the input pump polarization angles used in experiments as either tangential (T) to the exposed-core surface or perpendicular (P). The dashed yellow box in (a) corresponds to the image size of (b).

The experimental setup used to generate the third harmonic (TH) has been reported previously [25]. Briefly, ultrashort pulses of a 1560 nm femtosecond laser (Toptica, FemtoFiber pro IRS, 80 MHz, <40 fs pulses, average power 209 mW, 10 dB spectral bandwidth of approximately 200 nm – shown in Fig. 3b) were coupled into the core of a 40 mm length of ECF using an aspheric lens (Thorlabs, C230TM-C). In all experiments the ECF was fixed straight onto a stage to prevent bending or twisting. The input pump power and polarization were controlled using a combination of a rotating half wave plate and a polarizer. Except where otherwise stated, input light was polarized perpendicular (P) to the exposed-core surface (Fig. 1b). The ECF output was then coupled into a graded-index multi-mode fiber and fed into an optical spectrum analyzer (ANDO 6315A).

The measured output of the ECF at visible wavelengths for different coupled pump powers is shown in Fig. 2. Three distinct wavelengths were generated, showing that three different visible wavelength modes have phase-matched with the fundamental mode at IR pump wavelengths. The visible wavelength output has a cubic relationship with the input pump power, which is characteristic of THG.

Comparing the TH output from the 2.57 μm ECF used here to our previous results achieved with an ECF with a smaller core (1.85 μm) we see a 10.4 dB increase in the maximum output power (Fig. 3). The total integrated visible wavelength output power was 5.3 μW compared to the previous result of 0.96 μW. Given the average infrared pump power of 209 mW, this corresponds to total conversion efficiencies of 2.5×10^{-5} and 4.6×10^{-6} for the 2.57 μm and 1.85 μm ECFs, respectively.

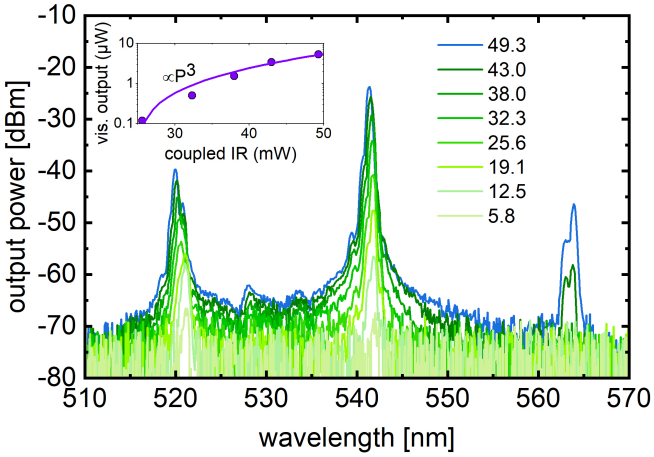

Fig. 2. Spectral distribution of the third harmonic output power at visible wavelengths measured from the exposed-core fiber (P-polarization, core diameter: 2.57 μm). Legend shows the transmitted (coupled) infrared average pump power (mW). The inset shows the accumulated visible output power obtained by integrating across the entire spectral range shown in the main plot as a function of coupled IR power.

The increased visible light emission is primarily due to three reasons: First, a larger transmitted (coupled) pump power was measured for the larger core (l) ECF (49.3 mW) compared to the smaller core (s) ECF (30.8 mW [25]). As unsaturated THG has a cubic relationship with the pump power, this can account for an increase of $K_\eta = (49.3/30.8)^3 = 4.1$.

Secondly, the larger core fiber also has comparatively lower optical loss. This is because losses associated with surface properties for an optical waveguide have a cubic relationship with the waveguide diameter [3] and the loss of the ECF is primarily determined by surface contamination of the exposed core. Therefore, the larger core ECF is expected to have loss a factor of $(2.57/1.85)^3 = 2.7$ times less than the smaller core fiber. This allowed a longer length of fiber to be used ($L_l = 40$ mm compared to $L_s = 3.3$ mm), noting that ultrafast THG will not scale proportionately with fiber length due to nonlinear phase accumulation and the associated dephasing of the fundamental mode at the fundamental frequency. Note that generally in the case of a longer fiber/waveguide the output TH-spectra are spectrally narrower since TH-signals are continuously generated at different local times while the pulse propagates down the fiber, which overall is a result of the mismatch of the group velocities of the fundamental and TH modes.

Finally, another factor that contributes to the improvement in TH-output power is the higher nonlinear coefficient of the large core ECF, which can be seen from the ratio of modal overlap between TH and fundamental waves: $J = \iint_{A_{NL}} (\hat{\mathbf{e}}_P^* \cdot \hat{\mathbf{e}}_P^*) \times (\hat{\mathbf{e}}_P^* \cdot \hat{\mathbf{e}}_{TH}) dxdy$ (details on ultra-fast THG can be

found in [30]). Here $\mathbf{e}_{TH}$ and $\mathbf{e}_{P}$ are the normalized electric fields of TH and fundamental wave, respectively and A_{NL} is the cross-section of the nonlinear material (silica). Since both ECFs are made from the same materials, the ratio between the two nonlinear coefficients, γ, only includes the ratio of the modal overlaps (that is, $\gamma \propto J$). Finite element simulations (COMSOL v5.2) were performed with geometries based on SEM images to estimate the modal overlap integrals. The visible wavelength mode with closest matching effective index and polarization (at 541 nm) to the fundamental IR wavelength mode (at 1623 nm) was found to have a modal overlap value of J_l = 0.0705 μm^{-2} for the 2.57 μm ECF, while only J_s = 0.0481 μm^{-2} for the 1.85 μm ECF (at 509 nm), giving rise to a nonlinear improvement factor of $K_\gamma = (J_l/J_s)^2$= 2.1 (cw-THG intensity has a square dependence on the nonlinear coefficient, that is, modal overlap). Note that the calculated modal overlaps highly depend on the exact spatial distributions of the modes involved in the phase-matching.

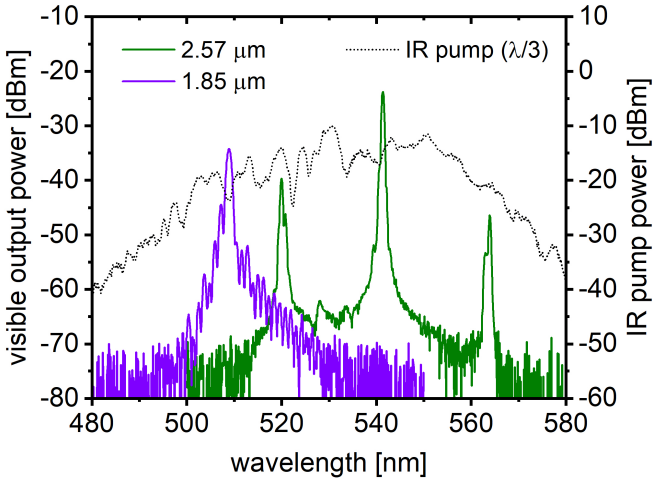

Fig. 3. Spectral distribution of the average third harmonic power for two ECFs with different core diameters (green: 2.57 μm, purple: 1.85 μm, P-polarization). The dotted black curve shows the corresponding infrared pump spectrum, at one-third of the IR wavelength. Note that the spectral measurements were optimized for visible wavelengths, thus the IR power (y-axis) cannot be correlated to the visible spectra.

Another parameter that can be used to control the generated wavelengths is the polarization orientation of the input beam. The sensitivity to input polarization is a result of the overlap integral (see previous equation), which is intrinsically sensitive to polarization via the scalar vector product between the pump and the TH modes. The particular magnitude of the overlap integral depends on the exact polarization properties of the phase-matched higher-order modes, which include complex multi-lobed spatial polarization distributions [25, 29].

The polarization dependence of THG from the 2.57 μm core diameter ECF was tested here by varying the linear input polarizer over 90 degrees. For each orientation the half-wave plate, which was located before the polarizer, was rotated to achieve maximum input IR pump power and thus maximum THG. The input IR pump power was consistent for each polarization orientation within the range of 47 mW to 51 mW. The generated visible wavelength spectra are shown in Fig. 4. It can be seen that the peaks previously observed in Fig. 2 at 520, 541 and 565 nm are present for the perpendicular polarization, but are greatly suppressed for the tangential (T) polarization. Meanwhile, new TH-peaks are present by rotating the polarization through to the T-polarization at wavelengths such as 511, 522, 529, 548, and 572 nm. The rich density of peaks in Fig. 4 shows the potential for customizing ultrafast visible light generation through design of a highly birefringent microstructured optical fiber and choice of input polarization.

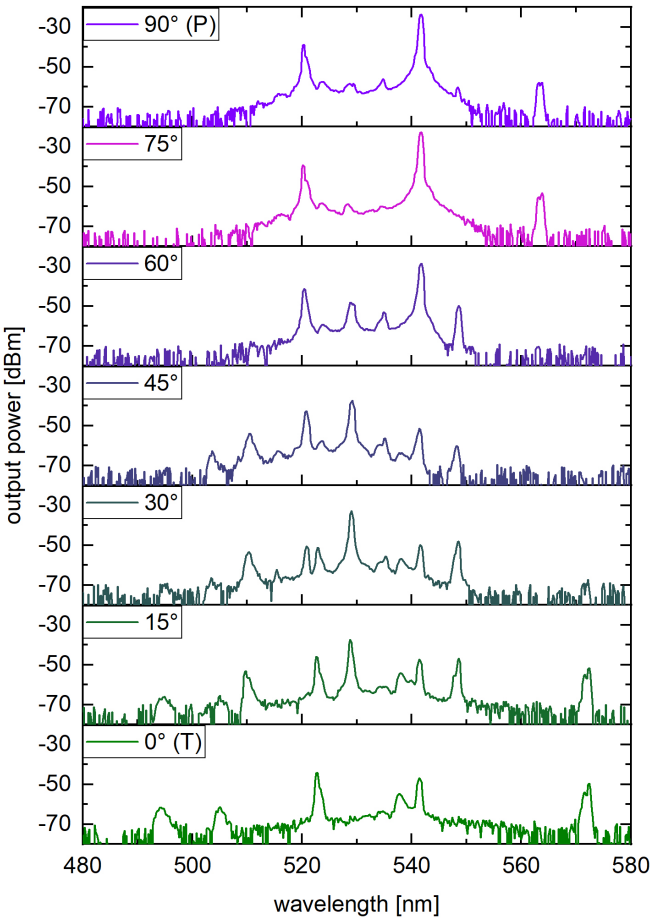

Fig. 4 Third harmonic generation from the exposed-core fiber (core diameter 2.57 μm) with varying angle of the input polarization. The legends refer to the respective polarization angle, where 0° (90°) refers to a polarization being tangential (perpendicular) to the surface of the exposed-core (defined in Fig. 1b).

Next to core diameter and input polarization, a third parameter that can be exploited for tuning THG from an ECF is modification of the evanescent field, and thus the effective mode index, through the deposition of dielectric nanofilms on the exposed core. We previously demonstrated that the phase-matching position of a single TH-mode could be shifted by up to 30 nm using a sputter coated Ta_2O_5 nanofilm [29]. Here we extend this experiment using the same parameters, but with the larger core diameter (2.57 μm) ECF, showing a different behavior compared to the previous work.

The results for 10 nm and 20 nm thick nanofilms are shown in Fig. 5. It is seen that the coating has a significant impact on the phase matching positions, with new wavelengths generated at 532

and 560 nm for the 10 nm coating and 542, 551 and 572 nm for the 20 nm coating. Unlike the results for the smaller core diameter fiber (1.85 μm), where we observed spectral shifting of a single TH-mode, there is no clear monotonic shift in the phase matching position. This is likely due to the dense number of modes supported by the larger core diameter fiber, which have complex patterns and polarization properties. Note that the modal distribution inside the nanofilm is different for the different modes, suggesting a spectral shifting behavior that is strongly correlated to the particular mode considered. Therefore, the distinct wavelengths present in Fig. 5 for the coated fiber do not represent phase-matching with the same modes in the uncoated fiber as it was reported for the small-core ECF.

While further analysis and characterisation is clearly needed to confirm the exact modes involved in phase-matching, the results clearly demonstrate the potential scope of nanofilm deposition on ECFs for generating tailorable third harmonics.

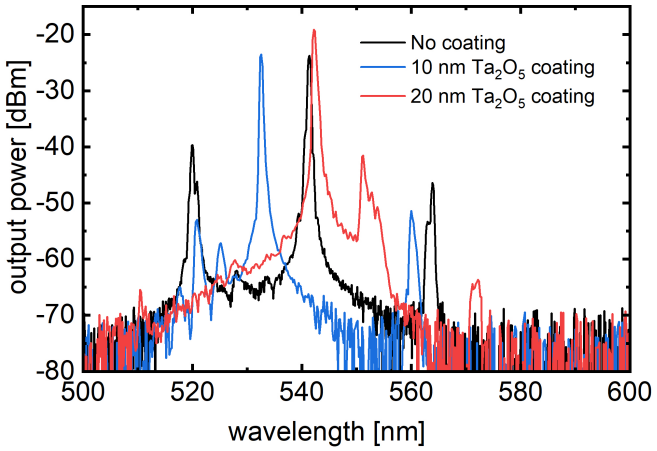

Fig. 5. Third harmonic generation from the ECF when the exposed core is coated with a Ta_2O_5 dielectric nanofilm. The various curves refer to different thicknesses of the nanofilm (black: no film; blue: 10nm; red: 20nm). Input polarization is perpendicular (P).

In this letter, multi-wavelength third harmonic generation has been demonstrated from an exposed-core microstructured optical fiber. By controlling core diameter, input pump polarization and depositing dielectric nanofilms onto the open core, various combinations of visible wavelength emission are possible, demonstrated here in the range of 495 to 570 nm. This provides a unique pathway towards tailored multi-wavelength ultrafast visible light sources for applications in sensing, microscopy, and quantum technologies.

Funding. European Commission through the Seventh Framework Programme (PIIF-GA-2013-623248). Ramsay Fellowship from the University of Adelaide. The OptoFab node of the Australian National Fabrication Facility utilizing Commonwealth and South Australian State Government funding. German Science Foundation (DFG, SCHM 2655/3-1). Free State of Thuringia (Fkz: 2015-0021). ARC Centre of Excellence for Nanoscale Biophotonics (CE14010003). Australian Research Council Linkage Project (LP150100657).

Acknowledgement. The authors thank Alastair Dowler and Evan Johnson for their contribution to the fiber fabrication.

References

1. S. Afshar V., W. Q. Zhang, H. Ebendorff-Heidepriem, and T. M. Monro, Opt. Lett. **34**, 3577-3579 (2009).
2. T. M. Monro, H. Ebendorff-Heidepriem, W. Q. Zhang, and S. Afshar V., IEEE J. Quantum Elect. **45**, 1357-1364 (2009).
3. H. Ebendorff-Heidepriem, S. C. Warren-Smith, and T. M. Monro, Opt. Express **17**, 2646-2657 (2009).
4. T. G. Euser, J. S. Y. Chen, M. Scharrer, P. S. J. Russell, N. J. Farrer, and P. J. Sadler, J. Appl. Phys. **103**, 103108 (2008).
5. L. Fu, B. K. Thomas, and L. Dong, Opt. Express **16**, 19629-19642 (2008).
6. O. Mouawad, J. Picot-Clémente, F. Amrani, C. Strutynski, J. Fatome, B. Kibler, F. Désévédavy, G. Gadret, J.-C. Jules, D. Deng, Y. Ohiski, and F. Smektala, Opt. Lett. **39**, 2684-2687 (2014).
7. W. Gao, M. El Amraoui, M. Laio, H. Kawashima, Z. Duan, D. Deng, T. Cheng, T. Suzuki, Y. Messaddeq, and Y. Ohishi, Opt. Express **21**, 9573-9583 (2013).
8. M. Szpulak and S. Février, IEEE Photonic. Tech. L. **21**, 884-886 (2009).
9. S. D. Le, D. M. Nguyen, M. Thual, L. Bramerie, M. C. e Silva, K. Lenglé, M. Gay, T. Chartier, L. Brilland, D. Méchin, P. Toupin, and J. Troles, Opt. Express **19**, B653-B660 (2011).
10. H. T. Munasinghe, A. Winterstein-Beckmann, C. Schiele, D. Manzani, L. Wondraczek, S. Afshar V., T. M. Monro, and H. Ebendorff-Heidepriem, Opt. Express **3**, 1488-1503 (2013).
11. M. I. M. A. Khudus, T. Lee, P. Horak, and G. Brambilla, Opt. Lett. **40**, 1318-1321 (2015).
12. T. Lee, Y. Jung, C. A. Codemard, M. Ding, N. G. R. Broderick, and G. Brambilla, Opt. Express **20**, 8503-8511 (2012).
13. A. Coillet and P. Grelu, Opt. Commun. **285**, 3493-3497 (2012).
14. V. Grubsky and J. Feinberg, Opt. Commun. **274**, 447-450 (2007).
15. A. Efimov, A. J. Taylor, F. G. Omenetto, J. C. Knight, W. J. Wadsworth, and P. S. J. Russell, Opt. Express **11**, 2567-2576 (2003).
16. F. G. Omenetto, A. Efimov, A. J. Taylor, J. C. Knight, W. J. Wadsworth, and P. S. J. Russell, Opt. Express **11**, 61-67 (2003).
17. S. Tsvetkov, K. Katamadze, N. Borshchevskaia, A. Sysolyatin, M. Fedorov, S. Kulik, M. Salganskii, and A. Belanov, Laser Phys. Lett. **13**, 025104 (2016).
18. K. Bencheikh, S. Richard, G. Mélin, G. Krabshuis, F. Gooijer, and J. A. Levenson, Opt. Lett. **37**, 289-291 (2012).
19. J. Hammer, A. Cavanna, R. Pennetta, M. V. Chekhova, P. S. J. Russell, and N. Y. Joly, Opt. Lett. **43**, 2320-2323 (2018).
20. J. Nold, P. Hölzer, N. Y. Joly, G. K. L. Wong, A. Nazarkin, A. Podlipensky, M. Scharrer, and P. S. J. Russell, Opt. Lett. **35**, 2922-2924 (2010).
21. X. Jiang, D. Zhang, T. Lee, and G. Brambilla, Opt. Lett. **43**, 2728-2731 (2018).
22. X. Jiang, T. Lee, J. He, M. I. M. A. Khudus, and G. Brambilla, Opt. Express **25**, 22626-22639 (2017).
23. Z. Montz and A. A. Ishaaya, Opt. Lett. **40**, 56-59 (2015).
24. A. Cavanna, F. Just, X. Jiang, G. Leuchs, M. V. Chekhova, P. S. J. Russell, and N. Y. Joly, Optica **3**, 952-955 (2016).
25. S. C. Warren-Smith, J. Wie, M. Chemnitz, R. Kostecki, H. Ebendorff-Heidepriem, T. M. Monro, and M. A. Schmidt, Opt. Express **24**, 17860-17867 (2016).
26. B. Doherty, M. Thiele, S. Warren-Smith, E. Schartner, H. Ebendorff-Heidepriem, W. Fritzsche, and M. A. Schmidt, Opt. Lett. **42**, 4395-4398 (2017).
27. R. Kostecki, H. Ebendorff-Heidepriem, S. C. Warren-Smith, and T. M. Monro, Opt. Mater. Express **4**, 29-40 (2014).
28. E. P. Schartner, A. Dowler, and H. Ebendorff-Heidepriem, Opt. Mater. Express **7**, 1496-1502 (2017).
29. S. C. Warren-Smith, M. Chemnitz, H. Schneidewind, R. Kostecki, H. Ebendorff-Heidepriem, T. M. Monro, and M. A. Schmidt, Opt. Lett. **42**, 1812-1815 (2017).
30. V. Grubsky and A. Savchenko, Opt. Express **13**, 6798-6806 (2005).

References – expanded list

1. S. Afshar V., W. Q. Zhang, H. Ebendorff-Heidepriem, and T. M. Monro, "Small core optical waveguides are more nonlinear than expected: experimental confirmation," Opt. Lett. **34**, 3577-3579 (2009).
2. T. M. Monro, H. Ebendorff-Heidepriem, W. Q. Zhang, and S. Afshar V., "Emerging nonlinear optical fibers: revised fundamentals, fabrication and access to extreme nonlinearity," IEEE J. Quantum Elect. **45**, 1357-1364 (2009).
3. H. Ebendorff-Heidepriem, S. C. Warren-Smith, and T. M. Monro, "Suspended nanowires: fabrication, design and characterization of fibers with nanoscale cores," Opt. Express **17**, 2646-2657 (2009).
4. T. G. Euser, J. S. Y. Chen, M. Scharrer, P. S. J. Russell, N. J. Farrer, and P. J. Sadler, "Quantitative broadband chemical sensing in air-suspended solid-core fibers," J. Appl. Phys. **103**, 103108 (2008).
5. L. Fu, B. K. Thomas, and L. Dong, "Efficient supercontinuum generations in silica suspended core fibers," Opt. Express **16**, 19629-19642 (2008).
6. O. Mouawad, J. Picot-Clémente, F. Amrani, C. Strutynski, J. Fatome, B. Kibler, F. Désévédavy, G. Gadret, J.-C. Jules, D. Deng, Y. Ohiski, and F. Smektala, "Multioctave midinfrared supercontinuum generation in suspended-core chalcogenide fibers," Opt. Lett. **39**, 2684-2687 (2014).
7. W. Gao, M. El Amraoui, M. Laio, H. Kawashima, Z. Duan, D. Deng, T. Cheng, T. Suzuki, Y. Messaddeq, and Y. Ohishi, "Mid-infrared supercontinuum generation in suspended-core As_2S_3 chalcogenide microstructured optical fiber," Opt. Express **21**, 9573-9583 (2013).
8. M. Szpulak and S. Février, "Chalcogenide As_2S_3 suspended core fiber for mid-IR wavelength conversion based on degenerate four-wave mixing," IEEE Photonic. Tech. L. **21**, 884-886 (2009).
9. S. D. Le, D. M. Nguyen, M. Thual, L. Bramerie, M. C. e Silva, K. Lenglé, M. Gay, T. Chartier, L. Brilland, D. Méchin, P. Toupin, and J. Troles, "Efficient four-wave mixing in an ultra-highly nonlinear suspended-core chalcogenide $As_{38}Se_{62}$ fiber " Opt. Express **19**, B653-B660 (2011).
10. H. T. Munasinghe, A. Winterstein-Beckmann, C. Schiele, D. Manzani, L. Wondraczek, S. Afshar V., T. M. Monro, and H. Ebendorff-Heidepriem, "Lead-germanate glasses and fibers: a practical alternative to tellurite for nonlinear fiber applications," Opt. Express **3**, 1488-1503 (2013).
11. M. I. M. A. Khudus, T. Lee, P. Horak, and G. Brambilla, "Effect of intrinsic surface roughness on the efficiency of intermodal phase matching in silica optical nanofibers," Opt. Lett. **40**, 1318-1321 (2015).
12. T. Lee, Y. Jung, C. A. Codemard, M. Ding, N. G. R. Broderick, and G. Brambilla, "Broadband third harmonic generation in tapered silica fibres," Opt. Express **20**, 8503-8511 (2012).
13. A. Coillet and P. Grelu, "Third-harmonic generation in optical microfibers: from silica experiments to highly nonlinear glass prospects," Opt. Commun. **285**, 3493-3497 (2012).
14. V. Grubsky and J. Feinberg, "Phase-matched third-harmonic UV generation using low-order modes in a glass micro-fiber," Opt. Commun. **274**, 447-450 (2007).
15. A. Efimov, A. J. Taylor, F. G. Omenetto, J. C. Knight, W. J. Wadsworth, and P. S. J. Russell, "Phase-matched third harmonic generation in microstructured fibers," Opt. Express **11**, 2567-2576 (2003).
16. F. G. Omenetto, A. Efimov, A. J. Taylor, J. C. Knight, W. J. Wadsworth, and P. S. J. Russell, "Polarization dependent harmonic generation in microstructured fibers," Opt. Express **11**, 61-67 (2003).
17. S. Tsvetkov, K. Katamadze, N. Borshchevskaia, A. Sysolyatin, M. Fedorov, S. Kulik, M. Salganskii, and A. Belanov, "Phase-matching of the HE_{11} and HE_{13} modes of highly doped GeO_2-SiO_2 fiber waveguides at 1596 nm and 532 nm, respectively, for triple-photon generation," Laser Phys. Lett. **13**, 025104 (2016).
18. K. Bencheikh, S. Richard, G. Mélin, G. Krabshuis, F. Gooijer, and J. A. Levenson, "Phase-matched third-harmonic generation in highly germanium-doped fiber," Opt. Lett. **37**, 289-291 (2012).
19. J. Hammer, A. Cavanna, R. Pennetta, M. V. Chekhova, P. S. J. Russell, and N. Y. Joly, "Dispersion tuning in sub-micron tapers for third-harmonic and photon triplet generation," Opt. Lett. **43**, 2320-2323 (2018).
20. J. Nold, P. Hölzer, N. Y. Joly, G. K. L. Wong, A. Nazarkin, A. Podlipensky, M. Scharrer, and P. S. J. Russell, "Pressure-controlled phase matching to third harmonic in Ar-filled hollow-core photonic crystal fiber," Opt. Lett. **35**, 2922-2924 (2010).
21. X. Jiang, D. Zhang, T. Lee, and G. Brambilla, "Optimized microfiber-based third-harmonic generation with adaptive control of phase mismatch," Opt. Lett. **43**, 2728-2731 (2018).
22. X. Jiang, T. Lee, J. He, M. I. M. A. Khudus, and G. Brambilla, "Fundamental-mode third harmonic generation in microfibers by pulse-induced quasi-phase matching," Opt. Express **25**, 22626-22639 (2017).
23. Z. Montz and A. A. Ishaaya, "Dual-bandgap hollow-core photonic crystal fibers for third harmonic generation," Opt. Lett. **40**, 56-59 (2015).
24. A. Cavanna, F. Just, X. Jiang, G. Leuchs, M. V. Chekhova, P. S. J. Russell, and N. Y. Joly, "Hybrid photonic-crystal fiber for single-mode phase matched generation of third harmonic and photon triplets," Optica **3**, 952-955 (2016).
25. S. C. Warren-Smith, J. Wie, M. Chemnitz, R. Kostecki, H. Ebendorff-Heidepriem, T. M. Monro, and M. A. Schmidt, "Third harmonic generation in exposed-core microstructured optical fibers," Opt. Express **24**, 17860-17867 (2016).
26. B. Doherty, M. Thiele, S. Warren-Smith, E. Schartner, H. Ebendorff-Heidepriem, W. Fritzsche, and M. A. Schmidt, "Plasmonic nanoparticle-functionalized exposed-core fiber—an optofluidic refractive index sensing platform," Opt. Lett. **42**, 4395-4398 (2017).
27. R. Kostecki, H. Ebendorff-Heidepriem, S. C. Warren-Smith, and T. M. Monro, "Predicting the drawing conditions for microstructured optical fiber fabrication," Opt. Mater. Express **4**, 29-40 (2014).
28. E. P. Schartner, A. Dowler, and H. Ebendorff-Heidepriem, "Fabrication of low-loss, small-core exposed core microstructured optical fibers," Opt. Mater. Express **7**, 1496-1502 (2017).
29. S. C. Warren-Smith, M. Chemnitz, H. Schneidewind, R. Kostecki, H. Ebendorff-Heidepriem, T. M. Monro, and M. A. Schmidt, "Nanofilm-induced spectral tuning of third harmonic generation," Opt. Lett. **42**, 1812-1815 (2017).
30. V. Grubsky and A. Savchenko, "Glass micro-fibers for efficient third harmonic generation," Opt. Express **13**, 6798-6806 (2005).